metals

MDPI

Article

Characteristic of Precipitate Evolution during High Temperature Annealing in Grain-Oriented Silicon Steel

Qian Gao [1,2,*], Jun Li [1,*], Xianhui Wang [2], Jian Gong [2] and Bo Li [1]

[1] China Iron and Steel Research Institute Group, Beijing 100081, China; lib@cisri.com.cn
[2] Shougang Zhixin Qian'an Electromagnetic Material Co., Ltd., Qian'an 064404, China; wangxianhui@sgqg.com (X.W.); gongjian@sgqg.com (J.G.)
* Correspondence: gaoqian@sgqg.com (Q.G.); junli@atmcn.com (J.L.)

Abstract: Precipitate evolution during high temperature annealing plays an important role in the magnetic property of grain-oriented silicon steel but was rarely studied. Aluminum was one of the important components of precipitates. Grain-oriented silicon steels with three levels of aluminum content were prepared and the interrupted extraction experiments were carried out. The results showed that during high temperature annealing, the precipitates were polygonal with the main composition of (Al,Si)N. Both the distribution density and volume fraction of precipitates showed first increasing and then decreasing tendencies, while the precipitate size remained approximately constant at first and then increased. Aluminum had a significant effect on the density and volume fraction of precipitates, which resulted in different secondary recrystallization structures. A small amount of aluminum with 0.015 wt.% led to low precipitate density, resulting in a low onset secondary recrystallization temperature as well as a Goss texture with large deviation angles. With the aluminum content of 0.025 wt.%, the secondary recrystallization was developed exactly right in the optimum temperature range, resulting in a perfect magnetic property. When the aluminum content was overcommitted to 0.035 wt.%, Goss grains could not show the preferential growth advantage and the secondary recrystallization structure could not be well developed.

Keywords: grain-oriented silicon steel; high temperature annealing; precipitate; aluminum; secondary recrystallization; texture

Citation: Gao, Q.; Li, J.; Wang, X.; Gong, J.; Li, B. Characteristic of Precipitate Evolution during High Temperature Annealing in Grain-Oriented Silicon Steel. *Metals* **2022**, *12*, 824. https://doi.org/10.3390/met12050824

Academic Editors: Krzysztof Talaśka, Szymon Wojciechowski and Antoine Ferreira

Received: 27 March 2022
Accepted: 9 May 2022
Published: 11 May 2022

1. Introduction

Grain-oriented silicon steel is a kind of soft magnetic material, which is widely used in the power industry because of its low iron loss and high permeability [1,2]. The traditional manufacturing technology for grain-oriented silicon steel is the slab high temperature reheating method. The heating temperature needs to reach as high as 1400 °C, which has many disadvantages, such as high energy consumption, large burning loss, and serious edge cracks. In contrast, for the slab low temperature reheating method, the heating temperature is only about 1150 °C; it has, therefore, become a hot topic in research in recent years, because of its low production cost and high yield [3–5]. Inhibitors play an important role in the grain growth and magnetic property of grain-oriented silicon steel. For the slab low temperature reheating method, the second phase particles dominated by AlN are usually used as the intrinsic inhibitors to inhibit the growth of recrystallized grains, so as to obtain fine equiaxed grains. After the nitriding stage, nitrogen atoms are combined with aluminum atoms to form additional inhibitors. During the high temperature annealing, the intrinsic and the additional inhibitors can together effectively restrain the abnormal growth of all the primary recrystallized grains except for the Goss oriented ({110} <001>) grains at a specific temperature range, as a result, the Goss oriented grains grow abnormally and swallow up the small grains around them, thus forming a single sharp Goss texture and developing excellent magnetic properties [3,6–9].

As an important component of the AlN inhibitor in grain-oriented silicon steel, the aluminum element has already been known for its extremely narrow process window and the significant impact on magnetic properties. A large number of studies were carried out on the precipitation behavior of AlN inhibitors, most of which were concentrated on the hot rolling and normalizing annealing [10–14]. Studies on precipitates during high temperature annealing were also reported [15–18]. However, the evolution of precipitates in slab low temperature reheating grain-oriented silicon steel during high temperature annealing, and especially the influence of aluminum element on the precipitate evolution as well as the secondary recrystallization structures, were rarely reported [19]. In this paper, grain-oriented silicon steels with three different aluminum contents were prepared with the slab low temperature reheating method in the laboratory. The precipitate evolution as well as the metallography, texture, and magnetic properties during high temperature annealing were studied in detail. The effect of aluminum element on the precipitates as well as the magnetic property were analyzed.

2. Materials and Methods

Three temperatures of slab low temperature reheating grain-oriented silicon steel were smelted in a 15 kg vacuum induction furnace. The billets with the size of 210 mm × 120 mm × 40 mm were obtained by mold casting process. The main chemical compositions (mass fraction, %) of the billets were 3.12–3.14 Si, 0.062–0.064 C, 0.069–0.070 Mn, 0.046–0.048 S, 0.0088–0.0092 N, with acid soluble aluminum Als 0.015, 0.025 and 0.035, respectively. Except for Als, the contents of other elements were all similar. According to the aluminum contents from the least to the most, the samples were numbered S1, S2, and S3. The billets were heated to 1150 °C for 120 min and then hot rolled to a thickness of 2.3 mm. After the two-stage normalizing annealing at 1120 °C × 3 min and 950 °C × 3 min successively, the plates were then cold rolled to 0.30 mm. The decarburizing annealing of 840 °C × 100 s was carried out in the N_2 and H_2 mixed wet atmosphere, during which the carbon contents of the experimental materials were controlled below 0.0020%, followed by the nitriding annealing of 780 °C × 80 s in the $N_2 + H_2 + NH_3$ dry atmosphere. During the high temperature annealing, the samples were first heated to 950 °C at a heating rate of 20 °C/h, and then heated to 1200 °C at a heating rate of 10 °C/h. To study the evolution of microstructures and precipitates, the interrupted extraction experiments were carried out and a group of samples were taken out from the furnace every 10 °C.

The carbon contents of samples after decarburizing annealing were determined by the LECO CS600 infrared absorption carbon-sulfur analysis unit. The Leica company's DM5000M metallographic microscope (Qian'an, China) was used to observe the longitudinal section metallographs of the extracted samples. After grinding the rolling surface of the samples to a certain depth from the surface, the precipitates were extracted by the carbon extraction replica technique. Then the carbon film replicas were observed on the JEOL company's JEM-2100 transmission electron microscope (Beijing, China). The chemical composition and crystal structure of the precipitates were analyzed with an EDS (energy dispersive spectrometer) and area electron diffraction patterns were selected. The Zeiss company's supra 55 field emission scanning electron microscope (Qian'an, China) was used to analyze the size and quantity of precipitates, and 40 micrographs were randomly taken for each sample. The micro textures of the samples extracted at 1200 °C were tested by the EBSD attached on the scanning electron microscope while the macro textures were determined using the XPert X-ray diffractometer (Qian'an, China) made by Panalytical company. The B_8 (the magnetic polarization intensity under an 800 A/m magnetic field) values of samples extracted at 1200 °C were tested on the NIM-2000E magnetic property measuring instrument.

3. Results and Discussion

3.1. Metallography

The metallography of samples extracted during high temperature annealing are shown in Figure 1. For the decarburized steels, the carbon contents were all below 0.0020 wt.%. It can be seen in Figure 1 that the microstructure after the decarburizing and nitriding processing stages was single ferrite and none cementite was found in any area of the metallographs, which confirmed that the carbon atoms were very few after decarburizing annealing, and there was no area with a high carbon concentration along the thickness direction of strips. The equiaxed grains were fine and uniform, with the grain sizes revealing no difference along the whole thickness. During the high temperature annealing, the microstructures remained as single ferrite without phase transformation to austenite due to the ultra-low carbon contents of below 0.0020 wt.%.

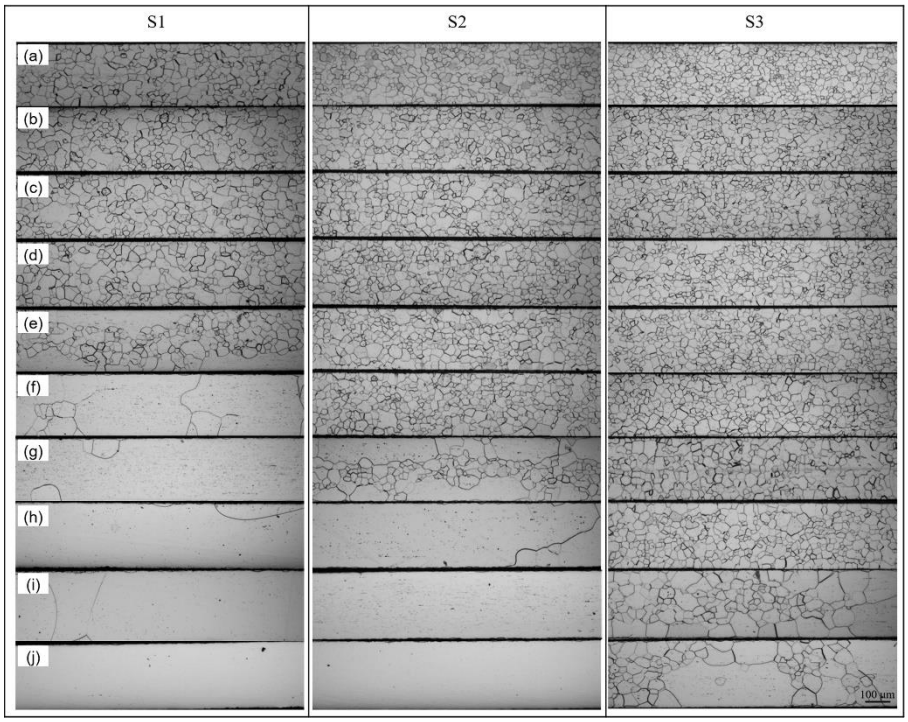

Figure 1. The metallography of the extracted samples during high temperature annealing. (**a**) 25 °C, (**b**) 850 °C; (**c**) 900 °C; (**d**) 980 °C; (**e**) 1000 °C; (**f**) 1010 °C; (**g**) 1020 °C; (**h**) 1030 °C; (**i**) 1040 °C; (**j**) 1200 °C.

For S1 steel, when the temperature increased to 980 °C, the microstructure remained uniform and the grains did not grow significantly, maintaining the average grain size of 23.2 μm. When the temperature reached 1000 °C, some grains near the surface started to devour the surrounding small grains and grow abnormally. With the further increase of temperature, the secondary recrystallization structure was developed into a much larger area and the whole viewing field was almost part of a large grain at 1020 °C. The equiaxed grains of S2 steel changed little until 1010 °C when the average grain size was 19.4 μm. The onset secondary recrystallization temperature was 1020 °C. At 1030 °C, the secondary recrystallization structure had been completely developed and the secondary grains had reached both the upper and lower surface of the sample. It took a longer time for the S2 steel to start abnormal growth than the S1 steel. For the S3 steel, when the temperature was up to 1030 °C, the metallography was still nearly the same as just after decarburizing and nitriding, with the average grain size of 17.3 μm. When the temperature rose to 1040 °C, the surface grains had grown to 80 μm, while the size of grains in the center layer was only close to 30 μm. Even when the temperature reached 1200 °C, the secondary recrystallization structure of S3 steel had not yet been well developed. Only a few grains grew to the size

of 100~300 μm and reached one or two surfaces of the sample, meanwhile the sizes of most grains were still about 30 μm. The microstructure of S3 steel failed to enter the steady growing stage for the secondary grains. The results indicated that the onset secondary recrystallization temperature went up with the increase of aluminum content, but when the aluminum content reached up to 0.035 wt.%, the onset secondary recrystallization temperature would be too high to develop a final secondary recrystallization structure.

It can also be seen from Figure 1 that the abnormal growth usually started on the surface and the grains grew faster sideways than into the thickness direction. First, during the high temperature annealing, the Ostwald ripening started earlier in the surface layer than the center layer, with the result that the pinning force on grain boundaries of sideways was much weaker than into the thickness direction. Second, the surface energy of the experimental steels were very high. Grain growth in the surface layer could reduce crystal defects such as grain boundaries and decrease the surface energy. The (110) plane of Goss oriented grains was the close-packed plane for the face-centered cubic structure, so when it was used as surface, the surface energy could also be reduced. According to the lowest energy principle, it was easier for the grains in the surface layer especially with (110) plane to grow sideways. Based on these factors, the growth rate of the abnormal growing grains was anisotropic.

3.2. Magnetic Property and Texture

The B_8 values of S1, S2 and S3 steels extracted at 1200 °C were 1.78 T, 1.94 T and 1.52 T, respectively. The EBSD orientation maps and pole figures of samples extracted at 1200 °C are shown in Figure 2. A single Goss texture was developed for both S1 and S2 steels, but the deviation angles of S1 steel from the exact Goss orientation were obviously larger than that of the S2 steel, which indicated that when the onset secondary recrystallization temperature was higher, the Goss texture would be more precise and the magnetic property would be better. For the S3 steel, the grains did not reveal a single Goss texture but several different orientations, such as {114}<481> (green), {100}<021> (purple) and {210}<001> (pink), which indicated that the secondary recrystallization structure could not be developed due to the competition between grains with different orientations, resulting finally in a poor magnetic property.

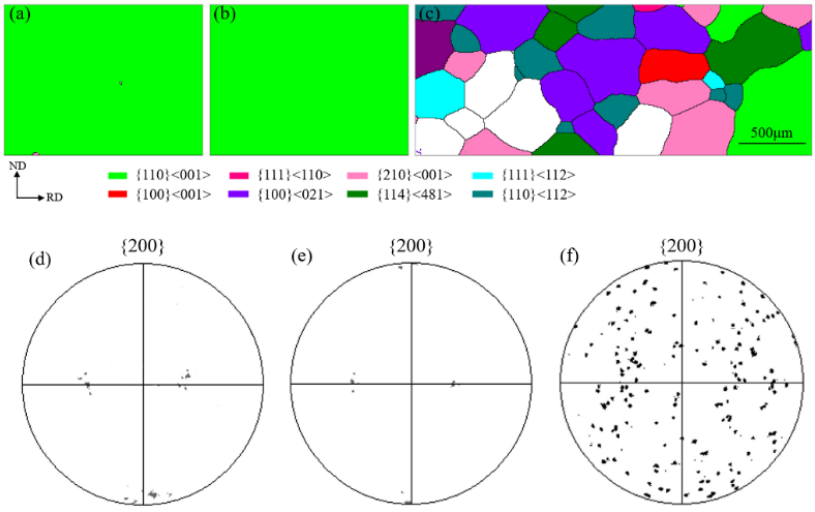

Figure 2. EBSD orientation maps and pole figures of samples extracted at 1200 °C. (**a**,**d**) S1 steel; (**b**,**e**) S2 steel; (**c**,**f**) S3 steel.

For the S1 and S2 steels extracted at 1200 °C, the secondary grains were so large in size that only using EBSD for micro textures characterization was not enough, thus the macro textures were further analyzed by XRD to observe the orientations of more grains. Several samples were stacked together and the longitudinal sections were tested. The polar

figures of S1 and S2 steels detected by XRD are shown in Figure 3. It could be seen that both of them were mainly of Goss texture. For S1 steel, the deviation angles α and β from the precise Goss orientation were 10° and 7.5° respectively, while those of S2 steel were 0°and 2.5°, which indicated that the Goss orientation in S2 steel was more accurate.

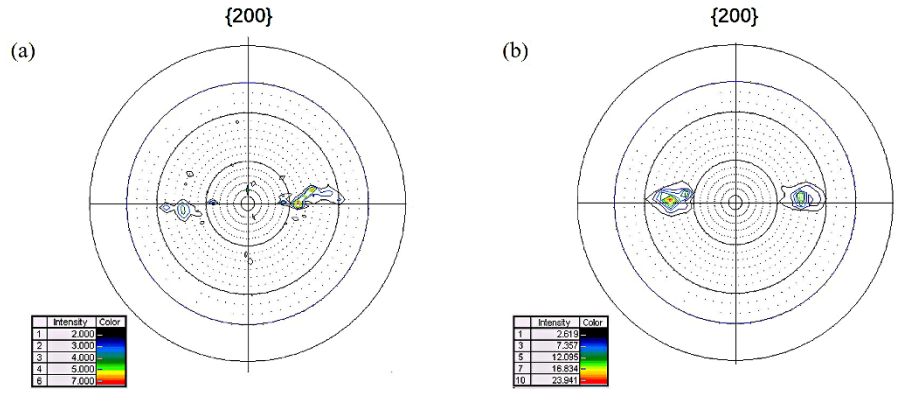

Figure 3. Polar figures detected by XRD for S1 steel (**a**) and S2 steel (**b**) extracted at 1200 °C.

3.3. Precipitate

After the nitriding processing of slab low temperature reheating grain-oriented silicon steel, the infiltrated nitrogen atoms distributed within 40 μm from the surface and reacted with the silicon steel matrix to form amorphous Si_3N_4 [16]. Moreover, the grain boundary diffusion for nitrogen atoms was much faster than the intracrystalline diffusion, so the Si_3N_4 was distributed more at grain boundaries than within grains. During high temperature annealing, nitrogen atoms at the surface grain boundaries diffused toward the inside of grains as well as the center layer of the samples, thus the unstable nitrides dissolved and precipitated into mid-thickness as (Al,Si)N with strong thermal stability in the temperature range from 750 °C to 900 °C [20].

On one hand, the nitrides were densely distributed in the surface layer just after nitriding and difficult to count, so precipitates in the surface layer were not suitable for characterizing that of the steel. On the other, due to the slow solidification rate in the center of the billets, many large size (1–5 μm) particles composed of AlN and MnS were precipitated and inherited to the center layer of the steel after being rolled, which could not act as effective inhibitors during the secondary recrystallization due to the large size; as a result, precipitates in the center layer were not fit for representing the steel either. Furthermore, the proportion of columnar crystals in the billets was more than 70%, where the component segregations of such elements as carbon, manganese, sulfur, and aluminum (although not prone to segregation) were weaker than in the central equiaxed crystals. The Goss crystal nuclei generally originated around the subsurface layer where only the columnar crystals zone in the billets was present, so precipitates near the Goss crystal nuclei played the most important role. As a result, precipitates at the position of 1/4 thickness from the surface were used as representation for each sample. The morphologies, electron diffraction patterns as well as the EDS spectra of precipitates in the S2 steel extracted at the temperatures of 980 °C and 1020 °C are shown in Figure 4.

It could be seen from Figure 4 that the precipitates were mainly polygonal with edges and corners. According to the EDS spectra and electron diffraction patterns, the main constituent of precipitates was (Al,Si)N with a hexagonal crystal structure and the proportion of MnS in the precipitates was very small. To count the precipitates more accurately, 40 micrographs were taken at the position of 1/4 thickness from the surface for each sample by SEM. The typical micrographs corresponding to the precipitate distributions of S1, S2, and S3 steels extracted at different temperatures are shown in Figure 5.

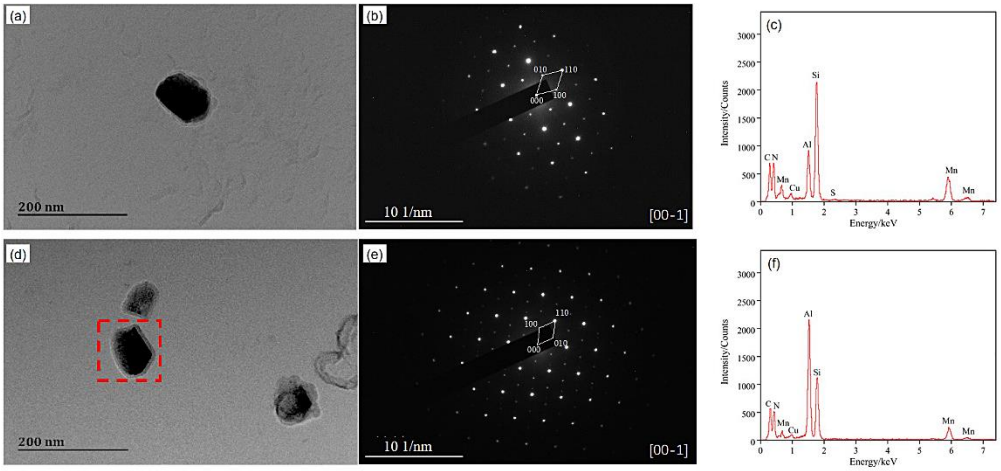

Figure 4. The morphologies, electron diffraction patterns and EDS spectra of precipitates in S2 steel extracted at 980 °C (**a**–**c**) and 1020 °C (**d**–**f**).

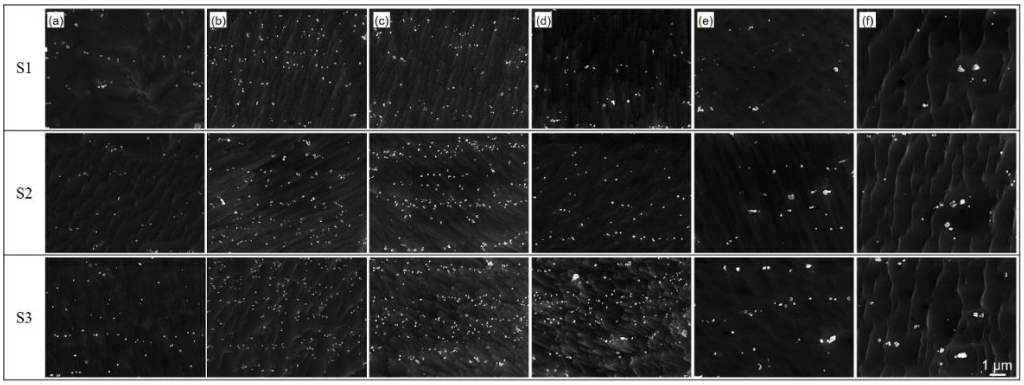

Figure 5. Typical micrographs corresponding to the precipitate distributions of samples extracted at different temperatures. (**a**) 850 °C; (**b**) 980 °C; (**c**) 1000 °C; (**d**) 1020 °C; (**e**) 1040 °C; (**f**) 1200 °C.

For all the micrographs, the average sizes as well as the distribution densities of precipitates were measured and the volume fractions were determined by the McCall-Boyd method shown in Equation (1) [17],

$$V_f = \left[\frac{1.4\pi}{6}\right] \cdot \left[\frac{ND_{mean}^3}{V}\right] \quad (1)$$

where N was the number of the second phase particles, D_{mean} was the mean diameter of the second phase particles, and V was the volume of the sample in which the second phase particles were located. Since the precipitates were exposed after the sample being eroded to a certain depth, the non-corroded steel matrix should not be included in the volume of the sample. The mean diameter of the precipitates was set as the thickness of the sample where the precipitates were located. Here, the area of each micrograph was expressed as S_p, then the volume of the sample in which the precipitates were located should be $40S_p$ multiplied by the D_{mean}. As a result, Equation (1) could be further transformed into Equation (2).

$$V_f = \left[\frac{1.4\pi}{240}\right] \cdot \left[\frac{ND_{mean}^2}{S_p}\right] \quad (2)$$

The results of the average diameter, distribution density, and volume fraction of precipitates in the extracted samples during high temperature annealing are shown in Figure 6. It could be seen that the trends of the distribution density and volume fraction of precipitates were basically the same during high temperature annealing, both of which

showed the first increasing and then decreasing tendencies. Meanwhile, the average diameter of precipitates remained approximately constant first and then increased. There were high concentrations of unstable nitrides in the surface layer of the samples while there were few nitrides in the inner layer just after nitriding. During the process of samples being heated, the nitrogen atoms in the surface layer diffused to the low concentration areas in the center layer through grain boundary diffusion and gap diffusion, reacted with the matrix alloy, and then precipitated uniformly and finely as (Al,Si) N, so that the volume fraction of precipitates at the position of 1/4 thickness from the surface layer kept increasing gradually until the distribution density of precipitates in the surface layer and the center layer tended to be the same. When the temperature increased from 850 °C to 980 °C, the volume fraction of precipitates in S1 steel increased from 0.23% to 0.62%. that of S2 steel increased from 0.29% to 1.20%, and that of S3 steel with the highest aluminum content increased from 0.34% to 1.36%, which indicated that the higher the aluminum content, the more precipitates were formed when the infiltrated nitrogen atoms had diffused into the center layer of the steel. Meanwhile, the average diameters of the precipitates in S1, S2, and S3 steels remained in the range of 75~85 nm.

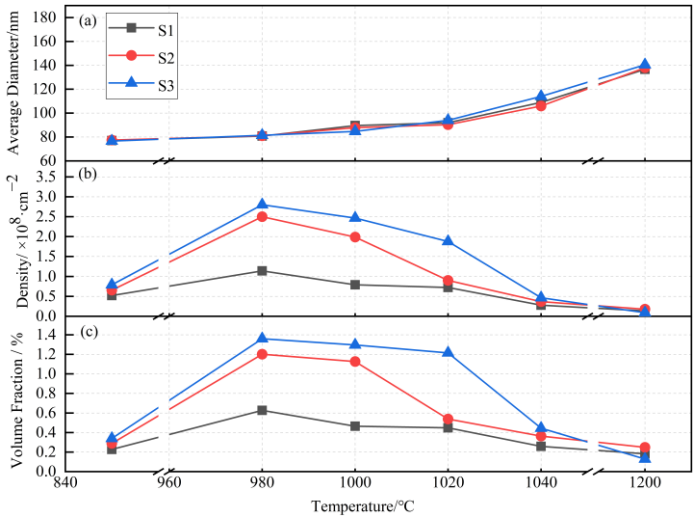

Figure 6. Statistics of precipitates in the extracted samples during high temperature annealing. (**a**) average diameter; (**b**) distribution density; (**c**) volume fraction.

From 1000 °C, the volume fractions of precipitates in the three samples all began to decrease, which indicated that the distribution density gradient of nitrides between the surface layer and the central layer decreased, and the diffusion velocity of nitrogen atoms along the thickness direction of the samples were significantly lower than the Ostwald ripening rate. During the process of the temperature increasing from 1000 °C to 1200 °C, small particles were dissolved into the matrix due to large curvature radius and precipitated again on the surface of the large particles, resulting in the reduced distribution density as well as the increased average diameter of precipitates.

The expression of ripening rate of the second phase particles $K_{(\Phi)}$ was shown in Equation (3) [21],

$$K_{(\Phi)} = \frac{A_{(\Phi)} D \Omega^2 \gamma C_e}{RT} \quad (3)$$

where $A_{(\Phi)}$ was the dimensionless constant directly proportional to the volume fraction Φ of the second phase particles, D was the diffusion coefficient, Ω was the amount of the second phase particles, γ was the interface energy, C_e was the equilibrium concentration of the second phase particles in the matrix, R was the gas constant, T was the absolute temperature. As can be seen from Equation (3), the ripening rate of precipitates accelerated with the increase of temperature due to the increase with temperature of the diffusion coefficient. Therefore, during the heating process, the ripening rate was faster when the temperature

was higher, but it was not a simple linear relationship as shown in Figure 6. Within the temperature range of 850~1040 °C, when the precipitates could be used as inhibitors, it could be seen from Equation (3) and Figure 6 that with the increase of aluminum content, the volume fraction of (Al,Si) N precipitates increased; as a result, the ripening rate of S1, S2 and S3 steels increased in turn. When the temperature increased to 1200 °C, the average diameters of the residual precipitates increased to 130~150 nm, and the volume fractions were less than 0.3% for all the samples. Figure 6 also shows that the aluminum content had little effect on the precipitate size at the same temperature.

According to the Gladman theory [22], when a certain critical size of inhibitors was reached, the pinning effect on grain boundaries would disappear. The unpinning of grain boundaries would increase the system energy, while the increase of grain size could effectively decrease the system energy, so the grains would grow up to achieve energy balance. The average diameter of precipitates in S1 steel reached 92 nm at 1000 °C, when the grain boundaries migrated rapidly and the secondary recrystallization was developed. For S2 steel, the average diameter of precipitates remained 91 nm at 1020 °C, which was near that of S1 at 1000 °C, but due to the higher volume fraction of precipitates, the secondary recrystallization was delayed being developed at 1020 °C. For S3 steel, the average diameter of precipitates at 1020 °C was 94 nm, which was similar to that of S2 steel at the same temperature. However, the volume fraction of precipitates in S3 steel was 1.21%, which was significantly higher than the 0.54% of S2 at the same temperature, so the secondary recrystallization still could not be developed at 1020 °C. When the volume fraction of precipitates in S3 steel dropped to below 0.54% at 1040 °C, the precipitate size had coarsened to 114 nm. Such coarsened precipitates made their inhibition function disappear and the secondary recrystallization development impossible. The explanation of such a phenomenon was explained in the following section.

3.4. Effect of Precipitate on Microstructure

Humphreys [23] proposed a dimensionless Z_H considering the Zener factor and primary grain size of precipitates to characterize the degree of grain growth, as shown in Equation (4),

$$Z_H = \frac{3fR}{2r} \tag{4}$$

where f was the volume fraction of the second phase particles, r was the average radius of the second phase particles, and R was the average radius of the recrystallized grains. According to the theory, if $0.1 < Z_H < 0.25$, it indicated normal and abnormal grain growth at the same time; if $0.2 < Z_H < 1$, it indicated abnormal grain growth but no normal grain growth; if $Z_H > 1$, there would be no grain growth. The Z_H values of the extracted samples during high temperature annealing are shown in Figure 7. Considering that the second phase particles would have no more inhibition effect on grain boundaries after the secondary recrystallization, the Z_H values of samples after secondary recrystallization were not listed in Figure 7.

From 850 °C to 980 °C, due to the diffusion of nitrogen atoms into the center layer and the precipitation of (Al,Si)N, the volume fraction of the precipitates increased, while the average radius of the recrystallized grains as well as the precipitates remained unchanged. As a result, the Z_H values of all the three samples increased. For S1 steel, the Z_H value was 1.18 at 980 °C, the volume fraction of precipitates was then as high as 0.63%, the pinning force was strong enough to restrain the migration of grain boundaries, as could be seen from Figure 1, there was no grain growth. During the process of temperature being increased to 1000 °C, the volume fraction of the precipitates decreased, thus the Z_H decreased to 0.90 due to the Ostwald ripening of precipitates, which weakened the grain boundary pinning force on the recrystallized grains. As a result, abnormal grain growth occurred due to grain boundary depinning. When the temperature rose to 1020 °C, all the grains had been developed into secondary recrystallization structure.

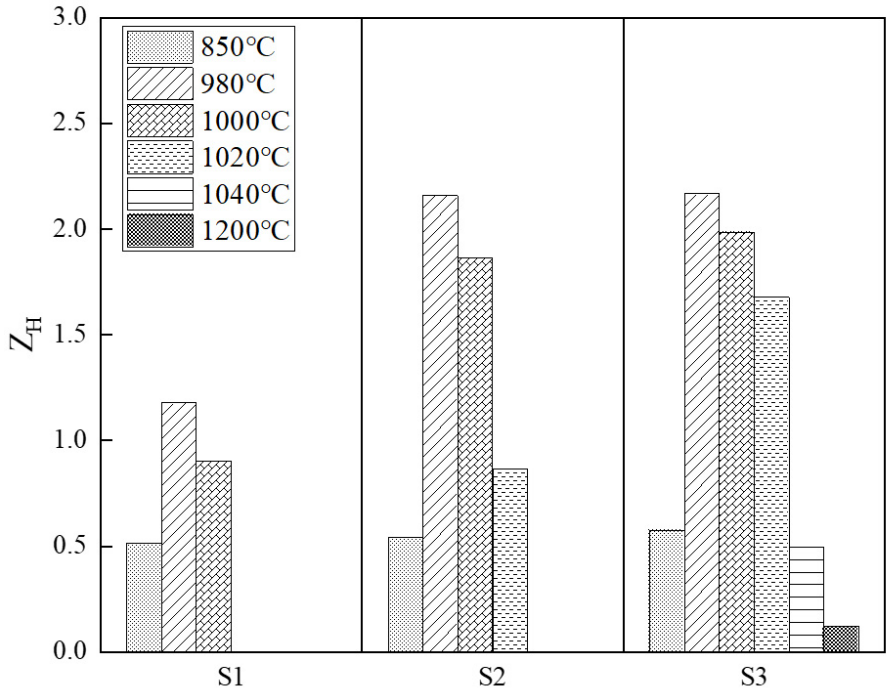

Figure 7. The Z_H values of the extracted samples during high temperature annealing.

The volume fraction of precipitates in S2 steel was higher than that of S1 at the same temperature. When the temperature increased from 980 °C to 1000 °C, the values of Z_H decreased from 2.2 to 1.9, but were still larger than 1, so no grain growth occurred. That was to say, with the increase of aluminum content, the pinning force of precipitates increased and the secondary recrystallization was delayed being developed at a higher temperature. It was reported that controlling the secondary recrystallization in a higher temperature range was beneficial to the sharp Goss texture [24–27]. When the temperature reached 1020 °C, the value of Z_H decreased to 0.87, which indicated the abnormal grain growth. When the temperature rose to 1030 °C, the grains had all been developed into secondary recrystallization structure.

At a temperature of 1020 °C, the secondary recrystallization structures of both S1 and S2 steels had been developed partly or totally. However, due to the high volume fraction, the Z_H value of S3 steel was still 1.68, and no grain growth occurred. The secondary recrystallization structure of S3 steel was not well developed during the high temperature annealing. The results at 1200 °C showed that the Z_H value decreased to 0.12, when the abnormal growth and normal growth occurred at the same time, which matched the metallograph in Figure 1 well. Some abnormally grown grains had been developed to the stable stage, for they had contacted both the upper and lower surface of the sample. A large number of primary recrystallized grains had increased from 17.3 μm to 30 μm. Therefore, it was indicated that both abnormal growth and normal growth occured at the same time. During the process of the Z_H value decreasing from 1.68 to 0.12, the range of $0.2 < Z_H < 1$ had been covered, when the secondary recrystallization structure should have been developed but actually not. It was because with the increase of temperature, the atom diffusion was accelerated, which promoted the dissolution of small particles and the coarsening of large particles. When the range $0.2 < Z_H < 1$ was reached, before developing the secondary recrystallization structure, the primary recrystallized grains had already grown up due to the rapidly reduced pinning force. Just as the metallograph shown of S3 steel at 1040 °C in Figure 1, though the Z_H of S3 steel was 0.51 at 1040 °C, the Goss oriented grains were unable to swallow up the growing grains around them, thus the secondary recrystallization structure could not be developed. It could be seen from above that aluminum content had an obvious effect on the pinning force of precipitates,

which directly affected the secondary recrystallization behavior. The accelerated ripening of precipitates at high temperature was the reason for incomplete secondary recrystallization.

4. Conclusions

1. The precipitates of slab low temperature reheating grain-oriented silicon steel during high temperature annealing were polygonal, the main composition of which was (Al,Si)N. Both the distribution density and volume fraction of precipitates showed increasing first before 980 °C and then decreasing tendencies, while the precipitate size remained approximately constant before 980 °C and then increased.
2. The microstructures after the decarburizing and nitriding processing stages were single ferrite equiaxed grains, with the consistent sizes along the thickness direction of the experimental materials. During the high temperature annealing, the microstructures remained as single ferrite without phase transformation to austenite due to the ultra-low carbon content of below 0.0020 wt.%.
3. The primary grain size remained almost unchanged before the onset secondary recrystallization temperature. Abnormal growth started from the surfaces and the growth rate was anisotropic. The appropriate onset temperature for secondary recrystallization ranged from 1000 °C to 1020 °C, when the Goss texture could be well developed and perfect magnetic property could be obtained.
4. The aluminum element had a significant effect on the distribution density and volume fraction of precipitates during high temperature annealing, which further affected the onset secondary recrystallization temperature as well as the magnetic property. The more the aluminum content, the higher the onset secondary recrystallization temperature and the better the magnetic property. However, when the aluminum content was as high as 0.035 wt.%, the excessive precipitates made Z_H quickly miss the range $0.2 < Z_H < 1$ which was suitable for secondary recrystallization, leading to both normal and abnormal grain growth, as a result, the secondary recrystallization structure could not be developed.

Author Contributions: Q.G.: Writing-original draft, investigation, formal analysis; J.L.: writing-review and editing, resources; X.W.: Project administration, investigation; B.L.: methodology, supervision; J.G.: conceptualization, supervision. All authors have read and agreed to the published version of the manuscript.

Funding: This research received no external funding.

Data Availability Statement: The data presented in this study are available upon request from the corresponding author.

Conflicts of Interest: The authors declare no conflict of interest.

References

1. Stoyka, V.; Kováč, F.; Stupakov, O.; Petryshynets, I. Texture evolution in Fe–3% Si steel treated under unconventional annealing conditions. *Mater. Charact.* **2010**, *61*, 1066–1073. [CrossRef]
2. Kubota, T.; Fujikura, M.; Ushigami, Y. Recent progress and future trend on grain-oriented silicon steel. *J. Magn. Magn. Mater.* **2000**, *215–216*, 69–73. [CrossRef]
3. Liao, C.C.; Hou, C.K. Effect of nitriding time on secondary recrystallization behaviors and magnetic properties of grain-oriented electrical steel. *J. Magn. Magn. Mater.* **2010**, *322*, 434–442. [CrossRef]
4. Kumano, T.; Haratani, T.; Fujll, N. Effect of nitriding on grain oriented silicon steel bearing aluminum. *ISIJ Int.* **2005**, *45*, 95–100. [CrossRef]
5. Xia, Z.; Kang, Y.; Wang, Q. Developments in the production of grain-oriented electrical steel. *J. Magn. Magn. Mater.* **2008**, *320*, 3229–3233. [CrossRef]
6. Wang, Y.; Zhu, C.; Li, G.; Liu, Y.; Liu, Y. Effect of decarburisation and nitriding on the carbon content, precipitates, microstructure and texture of Nb-bearing grain-oriented silicon steel. *Mater. High Temp.* **2020**, *37*, 155–164. [CrossRef]
7. Morawiec, A. On abnormal growth of Goss grains in grain-oriented silicon steel. *Scr. Mater.* **2011**, *64*, 466. [CrossRef]
8. Horký, P.; Pácl, P. Effective Grain Growth Inhibition in Silicon Steel. *J. Magn. Magn. Mater.* **1984**, *41*, 14–16. [CrossRef]

9. Song, H.Y.; Liu, H.T.; Lu, H.H.; An, L.Z.; Zhang, B.G.; Liu, W.Q.; Cao, G.M.; Li, C.G.; Liu, Z.Y.; Wang, G.D. Fabrication of grain-oriented silicon steel by a novel way: Strip casting process. *Mater. Lett.* **2014**, *137*, 475–478. [CrossRef]
10. Bao, S.; Xu, Y.; Zhao, G.; Huang, X.; Xiao, H.; Ye, C.; Song, N.; Chang, Q. Microstructure, texture and precipitates of grain-oriented silicon steel produced by thin slab casting and rolling process. *J. Iron Steel Res. Int.* **2017**, *24*, 91–96. [CrossRef]
11. Alcântara, F.L.D.; Barbosa, R.A.N.M.; Cunha, M.A.D. Aluminium nitride precipitation in Fe-3%Si steel. *ISIJ Int.* **2013**, *53*, 1211–1214. [CrossRef]
12. Ling, C.; Xiang, L.; Qiu, S.; Gan, Y. Effects of Normalizing annealing on grain-oriented silicon steel. *J. Iron Steel Res. Int.* **2014**, *21*, 690–694. [CrossRef]
13. Li, C.; Yang, H.; Wang, Y.; Yu, Y. Texture of Hot Rolled Strip for Fe-3Si Steel Produced by Thin Slab Casting and Rolling. *J. Iron Steel Res. Int.* **2010**, *17*, 46–53. [CrossRef]
14. Zhou, B.; Zhu, C.; Li, G.; Wan, X.; Schneider, J. Effect of Acid-Soluble Aluminum Content on Precipitates and Microstructure of Annealed Hot-Rolled Grain-Oriented Silicon Steel. *Steel Res. Int.* **2016**, *87*, 1702–1714. [CrossRef]
15. Fan, L.; Xiang, L.; Tang, G.; Qiu, S. Evolution of texture and precipitates in low temperature high magnetic induction grain-oriented silicon steel during high temperature annealing. *Funct. Mat.* **2013**, *44*, 3486–3491. [CrossRef]
16. Wu, Z.; Zhao, Y.; Li, J.; Li, B. Evolution of inhibitor in the annealing process at high temperature of low temperature hot roll and nitriding grain-oriented silicon steel. *Trans. Mater. Heat Treat.* **2011**, *32*, 84–87. [CrossRef]
17. Zhou, Y.; Xia, Z.; Wang, Q.; Xu, X.; Pan, L. Precipitating characteristics of inhibitors in grain-oriented electrical steel produced by low slab reheating temperature techniques during secondary recrystallization annealing. *Heat Treat. Met.* **2012**, *37*, 42–48. [CrossRef]
18. Zhu, Y.C.; Mao, J.H.; Wang, R.P.; Qiao, X.L. Effect of precipitated phase particles on secondary recrystallization in grain oriented silicon steel. *Heat Treat. Met.* **2009**, *34*, 29–32. [CrossRef]
19. Gao, Q.; Wang, X.; Li, J.; Gong, J.; Li, B. Effect of aluminum on secondary recrystallization texture and magnetic properties of grain-oriented silicon steel. *J. Iron Steel Res. Int.* **2021**, *28*, 479–487. [CrossRef]
20. Ushigami, Y.; Kurosawa, F.; Masui, H.; Suga, Y.; Takahashi, N. Precipitation behaviors of injected nitride inhibitors during secondary recrystallization annealing in grain oriented silicon steel. *Mater. Sci. Forum.* **1996**, *204–206*, 593–598. [CrossRef]
21. Marqusee, J.A.; Ross, J. Theory of Ostwald ripening: Competitive growth and its dependence on volume fraction. *J. Chem. Phys.* **1984**, *80*, 536. [CrossRef]
22. Gladman, T. On the Theory of the Effect of Precipitate Particles on Grain Growth in Metals. *Proc. R. Soc. Lond. A* **1966**, *294*, 298–309. [CrossRef]
23. Manohar, P.A.; Ferry, M.; Chandra, T. Five Decades of the Zener Equation. *ISIJ Int.* **1998**, *38*, 913–924. [CrossRef]
24. Kumano, T.; Ushigami, Y. Grain boundary characteristics of isolated grains in conventional grain oriented silicon steel. *ISIJ Int.* **2007**, *47*, 890–897. [CrossRef]
25. Lin, P.; Palumbo, G.; Harase, J.; Aust, K.T. Coincidence site lattice (CSL) grain boundaries and Goss texture development in Fe-3% Si alloy. *Acta Mater.* **1996**, *44*, 4677–4683. [CrossRef]
26. Shibayanagi, T.; Ichimiya, K.; Umakoshi, Y. Grain boundary migration in Fe-3mass% Si alloy bicrystals with twist boundary. *Sci. Technol. Adv. Mater.* **2000**, *1*, 87–95. [CrossRef]
27. Park, J.Y.; Han, K.S.; Woo, J.S.; Chang, S.K.; Rajmohan, N.; Szpunar, J.A. Influence of primary annealing condition on texture development in grain oriented electrical steels. *Acta Mater.* **2002**, *50*, 1825–1834. [CrossRef]